PCCP

Accepted Manuscript

ROYAL SOCIETY OF CHEMISTRY

www.rsc.org/pccp

PCCP

RSCPublishing

ARTICLE

Kinetic and mechanistic study of the reaction of OH radicals with methylated benzenes: 1,4-dimethyl-, 1,3,5-trimethyl-, 1,2,4,5-, 1,2,3,5- and 1,2,3,4-tetramethyl-, pentamethyl-, and hexa-methylbenzene

Cite this: DOI: 10.1039/x0xx00000x

Received 00th January 2012,
Accepted 00th January 2012

DOI: 10.1039/x0xx00000x

www.rsc.org/

P. Alarcon,[a] B. Bohn[b*] and C. Zetzsch[a,c]

The reaction of OH radicals with a series of methylated benzenes was studied in a temperature range 300−350 K using a flash-photolysis resonance fluorescence technique. Reversible OH additions led to complex OH decays dependent on the number of distinguishable adducts. Except for hexamethylbenzene, triexponential OH decay curves were obtained, consistent with formation of at least two adduct species. For three compounds that can strictly form two adduct isomers for symmetry reasons (1,4-dimethyl-, 1,3,5-trimethyl-, and 1,2,4,5-tetramethylbenzene) with OH bound *ortho* or *ipso* with respect to the methyl groups, OH decay curves were analysed in terms of a reaction mechanism in which the two adducts can be formed directly by OH addition or indirectly by isomerization. In all cases one adduct (add_1) is dominating the decomposition back to OH. The other (add_2) is more elusive and only detectable at elevated temperatures, similar to the single OH adduct of hexamethylbenzene. Two limiting cases of the general reaction mechanism could be examined quantitatively: reversible formation of add_2 exclusively in the OH reaction or by isomerization of add_1. Total OH rate constants, adduct loss rate constants and products of forward and reverse rate constants of reversible reactions were determined. From these quantities, adduct yields, equilibrium constants, as well as reaction enthalpies and entropies were derived for the three aromatics. Adduct yields strongly depend on the selected reaction model but generally formation of add_1 predominates. For both models equilibrium constants of OH reactions lie between those of OH + benzene from the literature and those obtained for OH + hexamethylbenzene. The corresponding reaction enthalpies of add_1 and add_2 formations are in a range –87±20 kJ mol^{-1}, less exothermic than for hexamethylbenzene (–101 kJ mol^{-1}). Reaction enthalpies of possible $add_1 \rightarrow add_2$ isomerizations are comparatively small. Because results for 1,3,5-trimethylbenzene are partly inconsistent with a direct formation of add_2, we promote the existence of isomerization reactions. Moreover, based on available theoretical work in the literature, add_1 and add_2 are tentatively identified as *ortho* and *ipso* adducts, respectively. Total OH rate constants were obtained for all title compounds. They can be described by Arrhenius equations: $k_{OH} = A \times \exp(-B/T)$. The parameters $\ln(A/(10^{-12}\text{cm}^3\text{s}^{-1}))$ = −25.6±0.3, −25.3±0.6, −27.3±0.3, −24.6±0.3, −26.2±0.4, −26.2±0.4 and −24.5±0.2, and B/K = −160±90, −550±180, −1120±90, −330±100, −820±100, −980±130, and −570±40 were determined for 1,4-dimethyl-, 1,3,5-trimethyl-, 1,2,4,5-, 1,2,3,5- and 1,2,3,4-tetramethyl-, pentamethyl-, and hexamethylbenzene.

Introduction

Atmospheric degradation of aromatic compounds is initiated to a large extent by OH radicals.[1-3] At room temperature and below, OH addition is the prevailing reaction channel for benzene and its methylated and poly-methylated derivatives. At higher temperatures, the addition becomes more and more reversible, and the competing abstraction of an H atom from the methyl groups (leading to an irreversible loss of OH) gains importance. However at tropospheric temperatures,

H abstraction is generally of minor importance[2] and back-decomposition is negligible at atmospheric O_2 concentrations because of competing adduct + O_2 reactions.[4,5] Nevertheless, the reversibility of adduct formation was utilized in the laboratory to study the reactive properties of OH-aromatics adducts and to obtain rate constants of atmospheric relevance.[4,5] Here we use the reversibility to investigate the formation and yields of possible adduct isomers that, together with the OH rate constants, are also important to understand the OH-initiated atmospheric degradation, as well as combustion processes at elevated temperatures.

In a system with pulsed production of OH in the presence of an excess of the aromatic, OH has been observed to disappear in a biexponential fashion.[4-6] The initial, fast OH decay is governed by the addition plus abstraction reaction while the final decay is determined by adduct decomposition back to OH and irreversible losses of OH and the adduct. Biexponential behaviour of decays has also been observed for OH in the presence of hexamethylbenzene (HMB, mellitene)[7] where all positions of the aromatic ring are occupied by methyl substituents This indicates formation of an *ipso*-adduct where OH is bound at an already occupied position. Berndt and Böge[8] found that the rate constant of the OH reaction with HMB was about 30 times greater than the expected rate constant for H-atom abstraction from a total of six methyl groups[2] demonstrating the importance of the *ipso* addition in the case of HMB. Further measurements by von Buttlar et al.,[9] and recently by Loison et al.,[10] confirmed the reversibility of the OH + HMB reaction, where formation of an ipso adduct is the only plausible reaction channel in the temperature range of these investigations.

Another interesting case is the addition of OH to 1,3,5-trimethylbenzene, where two addition channels are feasible: formation of an *ipso* adduct and an *ortho* adduct (at three equivalent positions each). Bohn and Zetzsch[11] investigated the reversible OH addition to this aromatic compound and observed triexponential OH decay curves, consistent with the formation of two distinguishable adduct species. However, the interpretation of the experimental data turned out to be difficult because two possible mechanisms for the formation of the second adduct – via OH reaction and isomerization – were found to lead to the same triexponential OH decays. Based on thermochemical reasons, a slow formation of the more stable adduct via isomerisation was tentatively favoured and assigned to the *ipso* adduct of 1,3,5-trimethylbenzene in analogy to the very stable *ipso* adduct of HMB.[9] Another result of this previous study[11] was that the use of the simpler single-adduct reaction model led to presumably wrong, smaller OH rate constants above room temperature. This finding is generally applicable to all aromatic compounds that can form more than one adduct species, as demonstrated for 1,2,3-trimethylbenzene and 1,2,4-trimethylbenzene[11] and more recently also for 1-methyl-4-isopropylbenzene (*p*-cymene).[12]

In this work, using the VUV flash-photolysis/resonance-fluorescence (FP-RF) technique, we investigated and reinvestigated the temperature dependent OH-decay kinetics for three aromatic compounds where the two-adduct reaction model should hold strictly for symmetry reasons: 1,4-dimethylbenzene (14-DMB, *p*-xylene), 1,3,5-trimethylbenzene (135-TMB, mesitylene) and 1,2,4,5-tetramethylbenzene (1245-TeMB, durene) in an attempt to further elucidate the underlying mechanism. Moreover, based on the simpler, single-adduct model, previously obtained experimental data with HMB[9] were re-evaluated, and former benzene results from our laboratory[4] were consulted for direct comparison. In addition, though not strictly applicable because of a greater number of possible adducts, the two-adduct approach was applied to derive best estimates of temperature dependent OH rate constants for the aromatic compounds 1,2,3,4-tetramethylbenzene (1234-TeMB, prehnitene), 1,2,3,5-tetramethylbenzene (1235-TeMB, isodurene) and pentamethylbenzene (PMB).

Experimental

The experimental setup used in this work has been described elsewhere.[5,6] OH radicals were generated by flash photolysis of water vapour, recently optimized using a Perkin Elmer FX 1165 short arc xenon flash lamp (flash energy 540 mJ) as VUV photolytic light source[12,13] with a MgF_2 window and improved trigger stability. A gas mixture of H_2O / He was allowed to flow through a resonance lamp, mounted at right angles to the VUV photolysis beam. A microwave discharge dissociated H_2O to produce electronically excited OH radicals. The radiation leaving the lamp was focused into the observation zone exciting the photolytically produced OH radicals in the reaction cell. The resonance fluorescence from the reaction cell passed through a 308 nm interference filter and was focused onto the photocathode of a photomultiplier tube (Thorn-EMI, 9789QB). The experiments were carried out under slow flow conditions in He. The procedure was fully automated by a PC with a software[5] that ran defined series of experiments at the desired temperature and total pressure unattended, triggering the flash lamp, collecting the fluorescence signals and saving the data from the multichannel scaler board (EG&G Ortec, model ACE MCS), as well as monitoring flow controllers, pressure gauges and platinum resistance thermometers to obtain a full set of the experimental data. Gas-phase concentrations of water and reactant were controlled by feeding known flows of He through saturators with water and the aromatic, adopting available Antoine constants from the literature and keeping the saturator for the aromatic compound precisely at the temperatures shown in Table S8 of the electronic supplementary information (ESI).

The initial OH radical concentration was estimated to be below 2×10^{10} cm^{-3} for a water concentration of 1.5×10^{15} cm^{-3}.[14] Based on a measured spectrum of the Xe flash lamp,[15] the initial concentration of OH, and VUV spectra from the literature,[16-18] the fractions of the aromatics that were photolysed were estimated to be below 6×10^{-4}. Because of the OH high reactivities of the aromatics this is not expected to influence the investigated OH decay kinetics, e.g. by radical +

radical reactions. Corresponding sensitivity tests using numerical simulations were made previously.[11]

Aromatics concentrations, temperatures and total pressures are presented in Table S1 and S2 (ESI). The gases used in this work had the following stated minimum purities: He (Riessner) – 99.996 %; N_2 (Linde) – 99.999 %. Deionised water was doubly distilled in a quartz still. Minimum purity for the aromatics was: liquid 14-DMB (Aldrich) 99 %; liquid 135-TMB (Janssen Chimica) 99%; solid 1245-TeMB (Aldrich) 98%, liquid 1234-TeMB (Chemos GmbH) 99.2%; liquid 1235-TeMB (prepared from the Grignard reaction of bromomesitylene[19]) 99% and solid PMB (Aldrich) 98%. 1245-TeMB and PMB were further purified by sublimation under vacuum at 70°C and 45°C, respectively.

Reaction model and data evaluation

The general reaction model that leads to triexponential OH decay curves in the presence of aromatics forming two adduct species was introduced recently.[11] It can be summarised by the following list of reactions with the corresponding rate constants given in parentheses:

OH + aromatic ↔ add_1	(k_{11a}, k_{-11a})	(R1)
OH + aromatic ↔ add_2	(k_{12a}, k_{-12a})	(R2)
add_1 ↔ add_2	(k_{12}, k_{21})	(R3)
OH + aromatic → products	(k_{1b})	(R4)
OH → products	(k_2)	(R5)
add_1 → products	(k_{31})	(R6)
add_2 → products	(k_{32})	(R7)

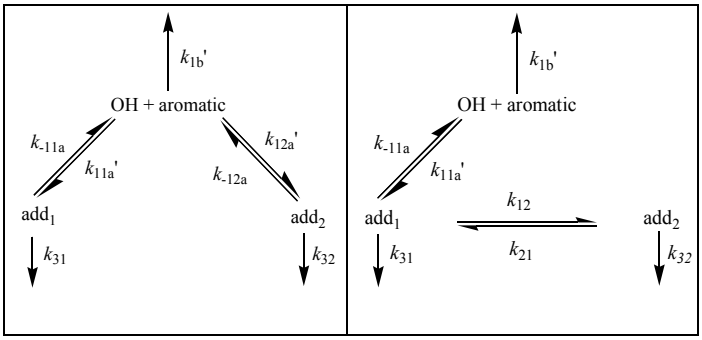

Fig. 1 Schematic diagrams of model-2 (left) and model-3 (right) for the OH radical addition to aromatic compounds. The $k_i' = k_i \times$ [aromatic] denote pseudo first-order rate constants of bimolecular reactions.

Reversible reactions R1-R3 represent redistributions between radical species that together with the loss processes determine the exact shape of the OH decays. Irreversible reactions R4-R7 are responsible for radical losses from the system, eventually leading to a decay of OH after its pulsed formation. The system of differential equations corresponding to R1-R7 was solved analytically for various starting conditions. These solutions were used to fit experimental OH decays and to determine the reaction rate constants indicated. Mathematical and technical details of the analytical solutions and the fitting procedures are given elsewhere.[11] A number of important aspects are repeated here to explain our approach:

(i) Sets of OH decay curves obtained at the same temperature but different aromatics concentrations were fitted simultaneously to improve the quality of fitted parameters. More details on concentration ranges and the number of decay curves used are given in the ESI.

(ii) The number of fit parameters is smaller than the number of rate constants involved in the mechanism and only certain sums and products of individual rate constants can be determined even by fitting sets of decay curves. The parameters are: k_2, $[k_{11a} + k_{12a} + k_{1b}]$, $[k_{11a}\, k_{-11a}]$, $[k_{12a}\, k_{-12a}]$, $[k_{12}\, k_{21}]$, $[k_{-11a} + k_{12} + k_{31}]$, and $[k_{-12a} + k_{21} + k_{32}]$. Where necessary, we put the combined quantities into square brackets to indicate that the rate constants within these brackets cannot be separated from each other.

(iii) A further complication arises because there is one more fit parameter than there are curve parameters describing a given set of triexponential decay curves. Consequently, different reaction mechanisms can lead to the same OH decay curves. We handle this problem by defining two limiting model cases where specific rate constants are set to zero. Two parameters, namely k_2 and $[k_{11a} + k_{12a} + k_{1b}]$, i.e., the total OH + aromatics rate constant, are not affected by this.

(iv) Uncertainties of fit parameters were estimated by rating the decrease of fit qualities upon a stepwise change of the parameters from the optimised values while allowing all other fit parameters to adjust. These uncertainty estimates also reflect the mutual dependencies of fit parameters, but they are not absolute and do not account for model deficiencies. Nevertheless, they are reasonable on a relative scale and are therefore suitable to weight data points in subsequent analyses, e.g. in Arrhenius fits.

In the following, three reaction models will be considered and fitted to experimental OH decay curves. Reaction model-2 and model-3 are shown schematically in Fig. 1.

Model-1: One adduct (biexponential OH decays). This can also be taken as a limiting case of the more general reaction model outlined above by setting $k_{12a} = [k_{12a}\, k_{-12a}] = 0$ and $k_{12} = [k_{12}\, k_{21}] = 0$. Model-1 will only be used to re-evaluate previously obtained data with HMB and to assess the improvements obtained in the fit qualities by applying the triexponential model for all investigated compounds.

Model-2: Two adducts (triexponential OH decays). No isomerization is permitted by setting $[k_{12}\, k_{21}] = 0$. Both adducts are exclusively formed in the OH reaction, so we also assume $k_{12} = k_{21} = 0$. By definition, add_1 is specified as the kinetically less stable adduct with the greater total loss rate constant, i.e. $k_{-11a} > k_{-12a}$. Both adducts decompose back to OH.

Model-3: Two adducts (triexponential OH decays). The kinetically more stable add_2 is assumed to be formed only by

isomerization by setting $[k_{12a}\,k_{-12a}] = 0$. Moreover, no dissociation of add_2 to OH is permitted, i.e. $k_{12a} = k_{-12a} = 0$ is a further assumption. Here add_2 also serves as a reservoir for OH, but only indirectly.

In addition, the following relationships (that generally apply for model-2, model-3 and any intermediate case) have been established previously:[11]

$$[k_{11a} + k_{12a} + k_{1b}] = k_{OH} = \text{const} \quad (1)$$

$$[k_{11a}k_{-11a}] + [k_{12a}k_{-12a}] = \text{const} \quad (2)$$

$$[k_{-11a} + k_{12} + k_{31}] \times [k_{-12a} + k_{21} + k_{32}] - [k_{12}k_{21}] = \text{const} \quad (3)$$

$$[k_{-11a} + k_{12} + k_{31}] + [k_{-12a} + k_{21} + k_{32}] = \text{const} \quad (4)$$

$$[k_{11a}k_{-11a}] \times [k_{-12a} + k_{21} + k_{32}] + [k_{12a}k_{-12a}] \times [k_{-11a} + k_{12} + k_{31}] + 2\sqrt{[k_{11a}k_{-11a}] \times [k_{12a}k_{-12a}] \times [k_{12}k_{21}]} = \text{const} \quad (5)$$

Results and discussion

Fit qualities and useful temperature range

A common feature, observed for benzene and all alkylated aromatics studied so far, is that OH regeneration is dominated by the presence of at least one quickly decomposing adduct species, whose decomposition rate constant increases from around 10 s^{-1} at 300 K to 200-400 s^{-1} at 350 K.[4-6,11,12,20] The only exception is HMB, where OH regeneration is negligible (<0.1 s^{-1}) at 300 K and only about 10 s^{-1} at 350 K.[9] As a consequence, OH decay curves for all other compounds investigated in this work are close to biexponential, and the presence of further, more stable adduct species is merely leading to small, but detectable deviations from a biexponential decay.

In order to check if the single-adduct model is sufficient to describe the OH decay curves or if the influence of a second adduct is noticeable, we determined the sum of squared residuals divided by the degrees of freedom (χ^2/DOF) for bi- and triexponential fits.[11] DOF is the total number of data points minus the number of fitted parameters. Figure 2 shows the obtained χ^2/DOF. Though negligible around room temperature, a clear decline of fit qualities towards greater temperatures was obtained for all compounds using biexponential fits. This indicates that in all cases there is evidence for the presence of more than one adduct species. Examples of bi- and triexponential fit curves obtained in the presence of 14-DMB are shown in Fig. S1 (ESI) under conditions with the greatest differences in fit qualities (334 K).

In contrast, for HMB the same χ^2/DOF were achieved in bi- and triexponential fits, independent of temperature in a reanalysis of experimental data by von Buttlar et al.[9] As expected, the same applies to data from an earlier work on benzene[21] that will not be discussed here any further.

A similar temperature dependence of fit qualities as shown in Fig. 2 has already been observed in previous work on TMB isomers[11] and *p*-cymene.[12,13] The common biexponential behaviour around room temperature and below is attributed to high stabilities of adduct species whose presence becomes noticeable only at elevated temperatures, as in the case of HMB. However, with increasing temperature also the decomposition rate constants of the kinetically less stable adducts increase exponentially, which makes it difficult to quantify the initial decay of OH overlapping with a high level of regenerated OH (eventually resulting in effective biexponential OH decays). This limits the range of useful temperatures, dependent on aromatics concentrations, experimental time resolution and decomposition rate constants. Under the conditions of this work these limits were reached between 340 and 360 K. Data analysis will therefore be confined to temperatures below these maxima. To make the OH decay curves triexponential at higher temperatures, much higher concentrations of aromatics would have to be used. Consequently, the initial OH decay would become extremely fast and the level of regenerated OH would go down. To monitor such OH decays requires an instrument with much higher time resolution and sensitivity than the one that was available in this work.

As mentioned in the introduction, 14-DMB, 135-TMB and 1245-TeMB can, because of their symmetry, add OH only at two positions: *ipso* and *ortho* with respect to the methyl groups. In these cases, the two-adduct model is expected to apply strictly, and a detailed data analysis is conducted in the following sections. The other three compounds, 1234-TeMB, 1235-TeMB, and PMB, can form three or four different adducts. For these compounds, despite similar fit qualities, triexponential OH decays are considered to be approximations, and therefore the data analysis was confined to the determination of OH rate constants. Because of the improved fit qualities, we expect these rate constants to be more reliable than those based on simpler models at least above room temperature. The same reasoning prompted a recent revision[11] of OH rate constants of 123-TMB and 124-TMB with regard to previously published parameterisations.[22]

OH + aromatics rate constants

The total OH + aromatics rate constants k_{OH} are direct parameters obtained by fitting arrays of OH decay curves. As outlined in the previous section, we used triexponential fits to determine the $k_{OH} = [k_{11a} + k_{12a} + k_{1b}]$, except for the reanalysis of HMB data[9] where the model-1 approach was applied. All temperature dependent k_{OH} are listed in Tables S3, S5 and S7 (ESI). Simple Arrhenius expressions were suitable to describe the temperature dependencies: $k_{OH} = A \times \exp(-B/T)$. In these fits, the k_{OH} were weighted by their estimated uncertainties as explained in section 3. Uncertainty estimates of the Arrhenius

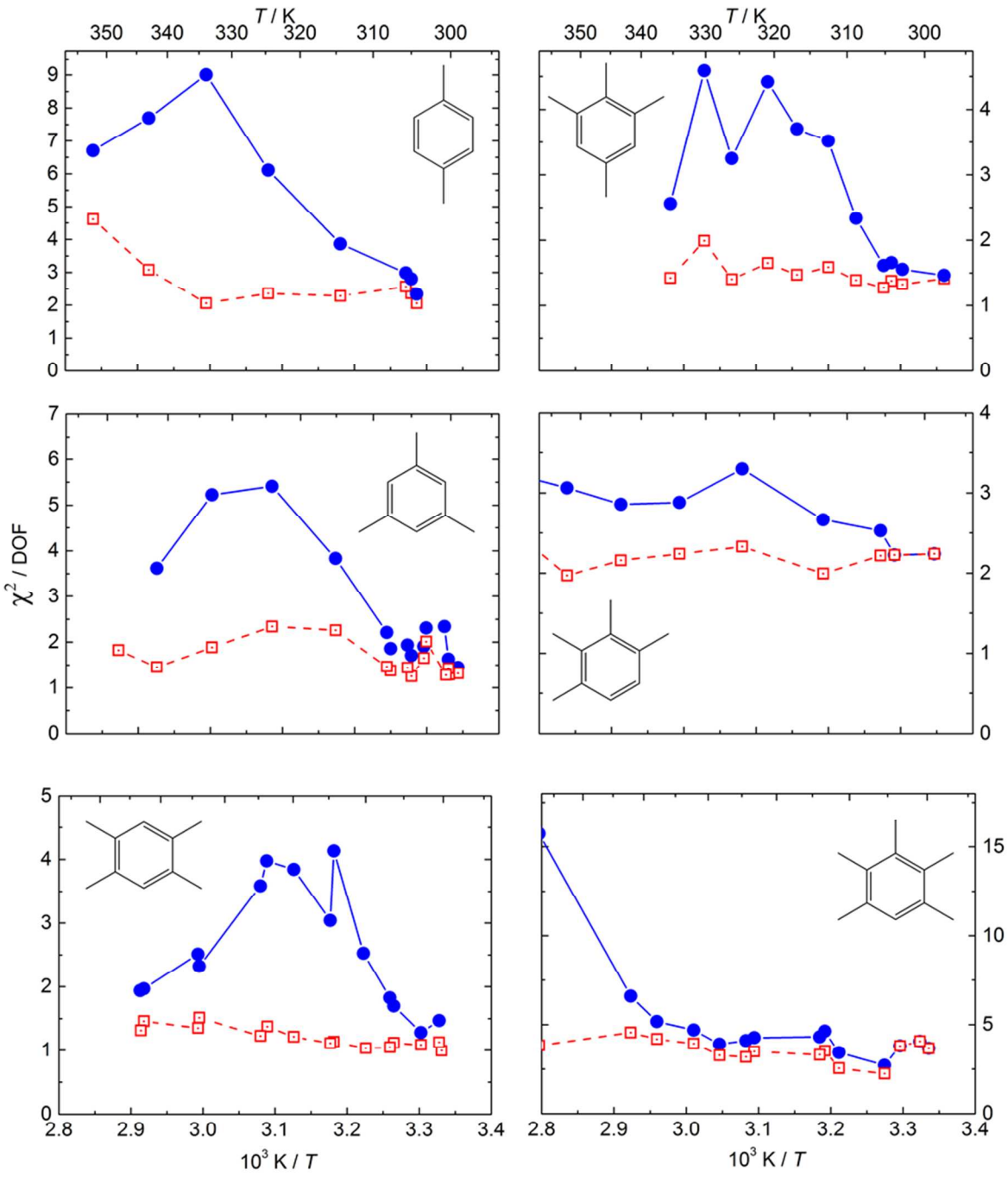

Fig. 2 Normalised residuals of biexponential fits (model-1, blue) and triexponential fits (model-2 or model-3, red) to arrays of OH decay curves in the presence of different aromatic compounds. Compounds on the left: two adducts possible. Compounds on the right: three and four adducts possible.

parameters A and B were derived using a Bootstrap method where the k_{OH} data sets were repeatedly (500 times) resampled using N randomly selected data points from the original set, also containing N data points. The standard deviations of the returned parameters A and B then define their estimated uncertainty.[23] For the parameters A, it turned out that the Bootstrap results were close to normal distributed on a logarithmic scale. Instead of the A themselves, we therefore report natural logarithms of A and their uncertainties. The bootstrap method is suitable when absolute uncertainties of single data points are poorly known, as is the case here. However, we consider these uncertainty estimates of A and B lower limits because the true T-dependence of k_{OH} could deviate from Arrhenius behaviour. Moreover, the k_{OH} also rely on the use of correct vapour pressures of the reactants that are documented in the ESI.

Table 1 presents room temperature k_{OH} and Arrhenius parameters compared with available literature data. In Figure 3,

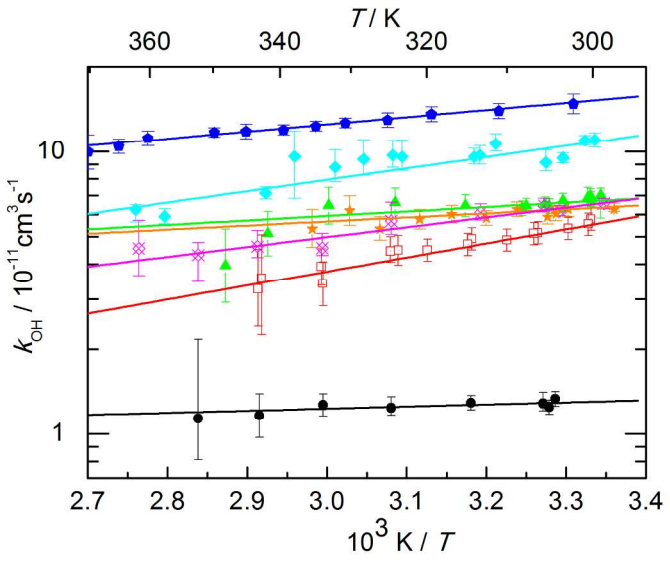

Fig. 3 Arrhenius plots of k_{OH} of methylated aromatic compounds and respective regression lines (Tab. 1). 14-DMB (filled circles), 1245-TeMB (open squares), 135-TMB (filled triangles), 1235-TeMB (filled asterisks), PMB (filled diamonds), 1234-TeMB (crossed diamonds), and HMB (filled pentagons).

all data are plotted as a function of temperature. Slightly negative activation energies were consistently obtained for the k_{OH} of all compounds indicating common formation of a pre-reactive complex, as predicted from DFT calculations for many aromatics,[12,24-29] including HMB.[10]

The k_{OH} generally increase with increasing methylation. For 14-DMB, the room temperature k_{OH} was found to be in good agreement with previous determinations that used absolute and relative methods (Tab. 1).

Arrhenius parameters derived from k_{OH} of a recent relative rate study with mass spectrometric detection of 14-DMB by Mehta et al.[30] also show good agreement with our results. The k_{OH} of 135-TMB led to a slightly weaker temperature dependence than in previous work from Aschmann et al.,[31] but in agreement with the work of Bohn and Zetzsch.[11] However, the k_{OH} of this work are greater by about 25%. Room temperature k_{OH} for 1245-TeMB and PMB are in good agreement with recent relative rate measurements by Aschmann et al.[32] at 298 K while for 1234-TeMB and 1235-TeMB no literature data are available. For HMB re-evaluated k_{OH} are very similar to those originally obtained by von Buttlar et al.,[9] as expected. The k_{OH} for HMB were the greatest of the compounds studied. The room temperature value is almost 40% greater than that determined by Berndt and Böge.[8] The reason for this discrepancy is unknown, but we note that HMB is difficult to handle because of an extremely low vapour pressure (see ESI for more details).

Model-dependent fit parameters

In contrast to the k_{OH}, all other fit parameters for 14-DMB, 135-TMB and 1245-TeMB depend on the reaction model as described in section 3. Regarding the parameters representing

Tab. 1 Total rate constants k_{OH} of the reaction OH + aromatic at room temperature and Arrhenius parameters A and B according to the equation: $k_{OH} = A \times \exp(-B/T)$ from the literature and this work. FP-RF: Flash photolysis – resonance fluorescence technique. RR: relative rate technique. Error limits of this work do not include potential systematic effects caused by deficiencies of reaction models or uncertainties of reactant concentrations (10-20%, see ESI).

	ln(A / cm^{3}s^{-1})	B /K	k_{OH}(298 K) /10^{-12} cm^{3}s^{-1}	Exper. Technique
14-DMB (p-xylene)			12.2 ± 1.2[33]	FP-RF
			10.7 ± 2.4[34]	RR
	−25.8 ± 1.6	−300 ± 500	15.3 ± 1.7[20]	FP-RF
			10.5 ± 1.0[35]	FP-RF
			13.5 ± 1.4[36]	FP-RF
			13.6 ± 0.6[37]	RR
			13.6[38]	RR
			13.0 ± 2.0[39]	RR
			14.7 ± 3.0[40]	RR
	−25.7 [a]	−150 [a]	11.9 ± 0.7[30]	RR
	−25.6±0.3 [b]	−160±90 [b]	13.1±0.3	FP-RF (this work)
135-TMB (mesitylene)			47.2 ± 4.8[33]	FP-RF
			44.4 ± 5.3[34]	RR
	−26.2 ± 3.2	−860 ± 1010	62.4 ± 7.5[20]	FP-RF
			40.9 ± 5.6[37]	RR
			57.5 ± 9.2[39]	RR
			57.3 ± 5.3[41]	RR
			59.1 ± 1.1[42]	RR
	−26.1	−740 ± 180	51.7 ± 1.1[31]	RR
	−25.1	−450 ± 50	59.5 ± 2.0[11]	FP-RF
	−25.3±0.6 [c]	−550±180 [c]	68.4±0.9	FP-RF (this work)
1245-TeMB (durene)			55.5 ± 3.4[32]	RR
	−27.3±0.3 [d]	−1120±90[d]	57.8±0.6	FP-RF (this work)
1235-TeMB (isodurene)	−24.6±0.3[e]	−330 ± 100 [e]	62.4 ± 0.8	FP-RF (this work)
1234-TeMB (prehnitene)	−26.2±0.4 [f]	−820 ± 100 [f]	66.4 ± 1.8	FP-RF
PMB			103 ± 8.0[32]	RR
	−26.2±0.4 [g]	−980 ± 130 [g]	110 ± 4	FP-RF (this work)
HMB (mellitene)			113 ± 11[8]	RR[i]
	−24.3	−498	149[9]	FP-RF
	−24.5±0.2 [h]	−570±40 [h]	153±2[9]	FP-RF (this work)

[a]Arrhenius parameter calculated from k_{OH} of indicated reference (240-340 K). Arrhenius parameter for the following temperature ranges (K): 304-352[b]; 299-348[c]; 300-343[d]; 297-335[e]; 298-362[f]; 299-362[g]; 311-370[h]. [i]295 K.

Tab. 2 Arrhenius parameters A and B of products of rate constants of forward and reverse reactions according to the equation: $k_F \times k_R = A \times \exp(-B/T)$. Error limits do not include potential systematic effects caused by deficiencies of reaction models.

	$\ln(A / \mathrm{cm^3\ s^{-2}})$	B / 10^3 K	$\ln(A / \mathrm{cm^3\ s^{-2}})$, $\ln(A / \mathrm{s^{-2}})$	B / 10^3 K
model-2	$k_{11a}k_{-11a}$		$k_{12a}k_{-12a}$	
14-DMB	4.2 ± 0.6	8.3 ± 0.2	−11.2 ± 1.3	4.3 ± 0.4
135-TMB	9.8 ± 1.6	9.5 ± 0.5	−28.5 ± 2.0	−1.6 ± 0.6
1245-TeMB	−0.3 ± 0.9	6.3 ± 0.3	2.7 ± 1.1	8.1 ± 0.3
model-3	$k_{11a}k_{-11a}$		$k_{12}k_{21}$	
14-DMB	3.6 ± 0.6	8.1 ± 0.2	42.9 ± 1.7	12.3 ± 0.5
135-TMB	8.4 ± 1.4	9.0 ± 0.4	27.0 ± 2.0	7.3 ± 0.6
1245-TeMB	0.3 ± 0.9	6.5 ± 0.3	51.7 ± 1.5	14.4 ± 0.5
model-1	$k_{11a}k_{-11a}$			
HMB	6.4 ± 0.2	9.45± 0.08	–	–

Tab. 3 Arrhenius parameters A and B of total adduct loss rate constants according to the equation: $k_L = A \times \exp(-B/T) + C$ of $\mathrm{add_1}$ (left), and $\mathrm{add_2}$ (right). The C parameters were held fixed. They correspond to optimized values according to equations (6) and (7) for model-2 and model-3, respectively. Error limits do not include potential systematic effects caused by deficiencies of reaction models.

	$\mathrm{add_1}$			$\mathrm{add_2}$		
	$\ln(A / \mathrm{s^{-1}})$	B / 10^3 K	C / $\mathrm{s^{-1}}$	$\ln(A / \mathrm{s^{-1}})$	B / 10^3 K	C / $\mathrm{s^{-1}}$
model-2						
14-DMB	29.0 ± 0.5	8.0 ± 0.2	4.1	23.0 ± 0.8	6.7 ± 0.3	1.3
135-TMB	31.0 ± 0.9	8.6 ± 0.3	3.9	18.3 ± 1.4	5.1 ± 0.4	1.2
1245-TeMB	30.1 ± 1.5	8.2 ± 0.5	22.8	28.5 ± 1.5	8.4 ± 0.5	2.5
model-3						
14-DMB	29.3 ± 0.5	8.2 ± 0.2	3.5	20.1 ± 1.1	5.7 ± 0.3	0.5
135-TMB	31.7 ± 0.8	8.9 ± 0.2	2.8	15.3 ± 1.3	4.1 ± 0.4	0.5
1245-TeMB	28.2 ± 1.2	7.5 ± 0.4	16.3	27.5 ± 1.3	7.9 ± 0.4	0.5
model-1						
benzene[a]	29.8 ± 0.8	8.6 ± 0.3	0.0	–	–	–
HMB	32.3 ± 0.5	10.4 ± 0.2	8.7	–	–	–

[a] Evaluated from k_R data by Knispel et al.,[4] $k_L = k_R$ + adduct background loss rate constant.

rate constant products, it turned out that the $[k_{12a}\,k_{-12a}]$ of model-2 were comparatively small while the $[k_{11a}\,k_{-11a}]$ were much greater. This demonstrates the dominance of $\mathrm{add_1}$ for the regeneration of OH for all compounds. However, the presence of $\mathrm{add_2}$ is not negligible as the $[k_{12a}\,k_{-12a}]$ of model-2 and the $[k_{12}\,k_{21}]$ of model-3 are all significantly greater than zero (fig. 4). Fitted rate constant products can be found in Table S3 and S4 (ESI). Note that equation (2) implies that the sum $[k_{11a}\,k_{-11a}]$ + $[k_{12a}\,k_{-12a}]$ of model-2 is identical to $[k_{11a}\,k_{-11a}]$ of model-3. Simple Arrhenius-type functions turned out to be suitable to describe the temperature dependencies of the rate constant products of forward (F) and reverse (R) reactions: $k_F \times k_R = A \times \exp(-B/T)$. The corresponding parameters A and B can be found in Table 2 including reevaluated model-1 results for HMB.[9] For model-2, positive temperature coefficients B were obtained for all $[k_{11a}\,k_{-11a}]$ and $[k_{12a}\,k_{-12a}]$ except for 135-TMB where for $[k_{12a}\,k_{-12a}]$ it was slightly negative in accordance with a previous investigation.[11] The parameters B for the rate constant products multiplied by the gas constant R represent the sum of activation energies of OH addition and reverse decomposition. This indicates that for $\mathrm{add_2}$ of 135-TMB the activation energy for the endothermic decomposition has to be over-compensated by a negative activation energy for OH addition, as will be confirmed in the next section. Given the generally weak, negative T-dependence of OH additions to aromatics, this possibility seems unrealistic. At least for 135-TMB model-2 is therefore equivocal. On the other hand, for model-3 positive temperature coefficients were obtained for the products $[k_{12}\,k_{21}]$, which is in qualitative agreement with expectations, i.e. positive sums of activation energies for potential isomerization reactions for all compounds (Fig. 5).

The remaining two fit parameters correspond to the total loss rate constants of $\mathrm{add_1}$ ($k_{-11a} + k_{12} + k_{31}$) and $\mathrm{add_2}$ ($k_{-12a} + k_{21} + k_{32}$). They represent a sum of two or three first-order rate constants, dependent on model assumptions (section 3). For all investigated compounds it was found that the loss rate constants of $\mathrm{add_2}$ were much smaller than those of $\mathrm{add_1}$ (Fig. 6). Model-2 and model-3 fits gave rather similar results for the two loss rate

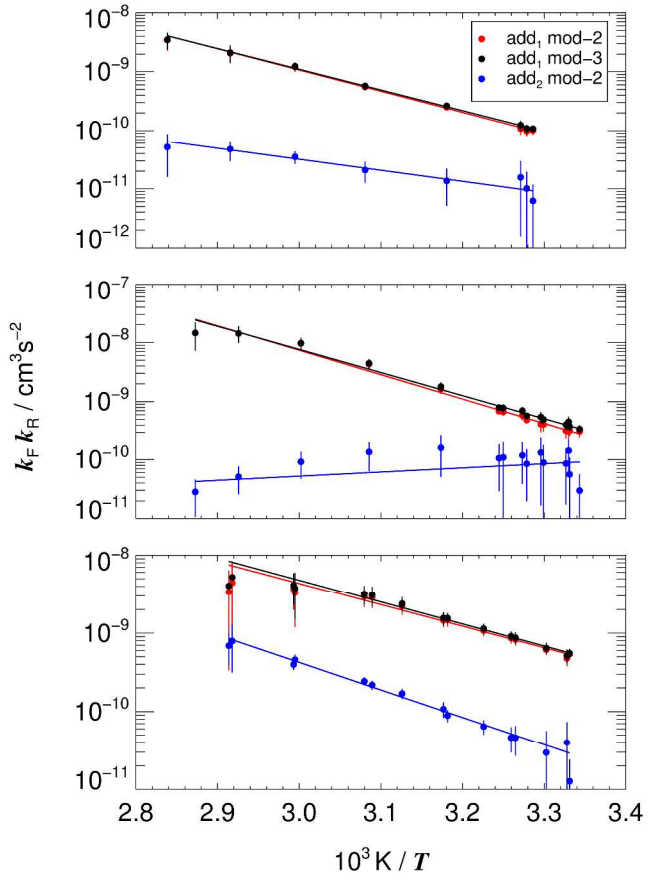

Fig. 4 Arrhenius plots of forward and reverse rate constant products $k_F\,k_R$ for 14-DMB (upper panel), 135-TMB (middle panel), and 1245-TeMB (lower panel). Black: [$k_{11a}\,k_{-11a}$] of model-3, red: [$k_{11a}\,k_{-11a}$] of model-2, and blue: [$k_{12a}\,k_{-12a}$] of model-2.

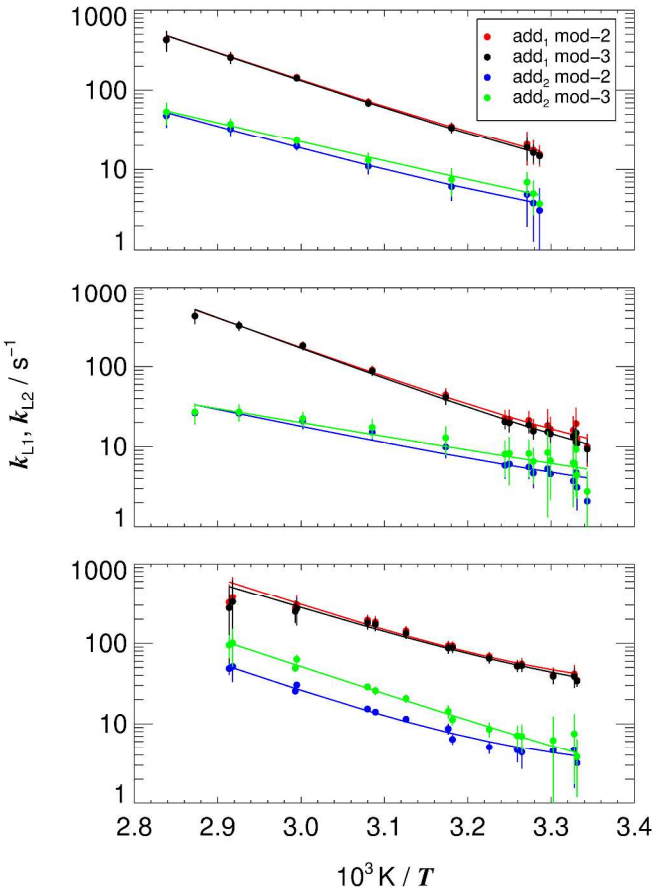

Fig. 6 Arrhenius plots of loss rate constants k_{L1} and k_{L2} of add_1 and add_2 for 14-DMB (upper panel), 135-TMB (middle panel), and 1245-TeMB (lower panel). Red: k_{L1} of model-2, black: k_{L1} of model-3, blue: k_{L2} of model-2, and green: k_{L2} of model-3.

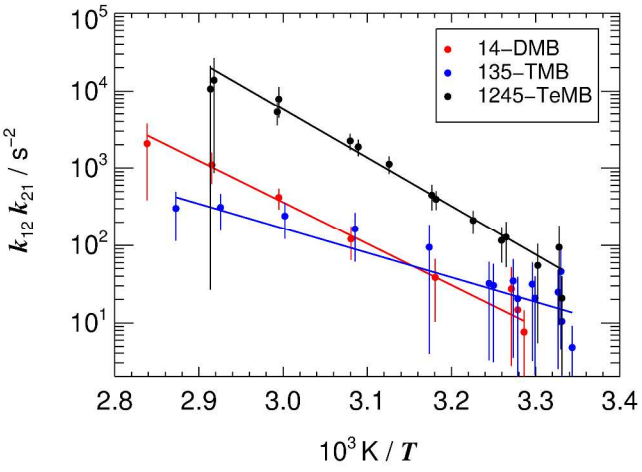

Fig. 5 Arrhenius plots of rate constant products [$k_{12}\,k_{21}$] of model-3 for 14-DMB (red), 135-TMB (blue), and 1245-TeMB (black).

constants. The differences were not significant for add_1 within estimated uncertainties. Loss rate constants are listed in Table S3 and S4 (ESI). Note that equation (4) indicates that the sum of all loss rate constants also has to be constant, independent of the reaction model.

The temperature dependence of the adduct-loss rate constants k_{L1} (add_1) and k_{L2} (add_2) can be described by a modified Arrhenius equation: $k_L = A \times \exp(-B/T) + C$. The parameters A, B and C are given in Table 3. Because the dependence of A and B on C is pronounced, in particular for add_2, the C were kept fixed at values that will be derived in the next section, based on OH budget considerations.

For model-2, the C should correspond to the background loss rate constants k_{31} and k_{32} that are assumed to be independent of temperature for convenience, i.e. $k_{L1} = [k_{-11a} + k_{31}]$ and $k_{L2} = [k_{-12a} + k_{32}]$. The temperature coefficients B multiplied by R correspond to the activation energies of adduct decompositions. They all range around 67−72 kJ mol^{-1} for add_1 dependent on compound, in good agreement with results for benzene by Perry et al.,[20] and Knispel et al.,[4] of (78±8) kJ mol^{-1}

and (72±2) kJ mol^{-1}, respectively. Similar results exist for other aromatic compounds[4,11,20] but they may be affected by the use of the wrong reaction model.[11] In contrast, the activation energy for the OH-HMB adduct is greater (89 kJ mol^{-1}). In recent work on 135-TMB,[11] a slightly greater activation energy for the decomposition of add$_1$ of 135-TMB of (81±9) kJ mol^{-1} was obtained, but still in the range of combined error estimates compared to the result of this work.

With one exception (1245-TeMB), the corresponding activation energies for add$_2$ are smaller, in particular for 135-TMB where it is unrealistically small for the decomposition reaction (43 kJ mol^{-1}). This has already been noted in earlier work[11] where a similar value was obtained and model-2 was therefore questioned for 135-TMB. However, it should be noted that because of the limited temperature range and the dependence on k_{32}, the parameters A and B for add$_2$ are particularly uncertain.

The only theoretical study on the investigated compounds that addressed the properties of *ortho* and *ipso* adducts was made by Fan and Zhang [27] on the OH + 14-DMB reaction based on reaction model-2. Although calculated decomposition rate constants at 300 K were greater by two orders of magnitude, the authors predicted that the *ortho* adduct decomposes a factor of 3.5 more rapidly than the *ipso* adduct. This is in qualitative agreement with this work if we identify add$_1$ and add$_2$ as *ortho* and *ipso* adducts, respectively.

For model-3 the situation is more complicated for add$_1$ and different for add$_2$: $k_{L1} = [k_{-11a} + k_{12} + k_{31}]$ and $k_{L2} = [k_{21} + k_{32}]$. A clear assignment of C to k_{31} is difficult here unless k_{-11a} and k_{12} accidentally have the same T-dependencies. However, the contribution of k_{12} to the total loss rate constant of add$_1$ is small, as will be shown in the next section, i.e. back decomposition remains the main loss process for add$_1$ also for model-3. Generally, similar A and B were obtained as for model-2 but the loss rate constants of add$_2$ now correspond to the sum $[k_{21} + k_{32}]$. Therefore the temperature dependence of k_{L2} reflects that of the isomerization rather than of a decomposition reaction which could explain the unexpectedly low value of the activation energy obtained for 135-TMB.

Adduct yields and background losses

The yields of add$_1$ and add$_2$ according to model-2, $\phi_1 = k_{11a}/k_{OH}$ and $\phi_2 = k_{12a}/k_{OH}$, can be determined from the obtained fit parameters utilizing the following equation:[11]

$$k_{OH} - k_{1b} = k_{11a} + k_{12a} = \frac{[k_{11a}k_{-11a}]}{k_{L1} - k_{31}} + \frac{[k_{12a}k_{-12a}]}{k_{L2} - k_{32}} \quad (6)$$

For the k_{1b}, a recommendation by Atkinson[2] was used (temperature dependent abstraction rate constant per CH_3 substituent), and background loss rate constants k_{31} and k_{32} were fitted using equation (6) (Tab. 3). The fits ensure that the OH budget is closed at least towards lower temperatures where k_{31} and k_{32} have significant influence. The background rate constants obtained this way compare reasonably with the empirical parameters C introduced in the last section but are preferred for the calculation of adduct yields for consistency reasons.

Correspondingly, the yield of add$_1$ according to model-3 can be determined using the following relation:[11]

$$k_{OH} - k_{1b} = k_{11a} = \frac{[k_{11a}k_{-11a}]}{k_{L1} - k_{12} - k_{31}}$$
$$= \frac{[k_{11a}k_{-11a}] \times (k_{L2} - k_{32})}{(k_{L1} - k_{31}) \times (k_{L2} - k_{32}) - [k_{12}k_{21}]} \quad (7)$$

Again the k_{31} and k_{32} for model-3 were fitted using equation (7). They were slightly smaller than those of model-2 (Tab. 3), but generally all adduct background loss rate constants ranged below 4 s^{-1} which is typical for the experimental setup used. The only exception is add$_1$ of 1245-TeMB where the k_{31} were 23 s^{-1} and 16 s^{-1} for model-2 and model-3, respectively. The reason for this increased background loss is unknown. It could be caused by an exceptionally large rate constant of a reaction of this adduct with traces of O_2 or by a specific unimolecular loss reaction.

Adduct yields, the contribution of H-abstraction, and corresponding total yields as a function of temperature are shown in Fig. 7. Total yields are close to unity in all cases, as expected. The ϕ_1 range between lower limits defined by model-2 and upper limits close to 0.9 according to model-3 (ϕ_2=0) while upper limits of ϕ_2 are defined by model-2. Unfortunately, the experimental OH decay data alone do not allow us to further confine these ranges. However, the 14-DMB results of model-2 are in reasonable agreement with a theoretically predicted 0.8 to 0.2 *ortho* to *ipso* branching ratio by Fan and Zhang[27] if we again assign add$_1$ and add$_2$ as *ortho* and *ipso* adducts, respectively. Regarding the model-2 temperature effect on adduct yields, only 135-TMB exhibits a strong dependence. The exponential decrease of ϕ_2 with temperature corresponds to the aforementioned unusually large negative temperature coefficient of add$_2$ formation by OH addition, also explaining the negative temperature coefficient of the product $[k_{12a}\, k_{-12a}]$ for 135-TMB.

Equilibrium constants and thermodynamic quantities

Ratios of rate constants of forward and reverse reactions were used to calculate equilibrium constants of reversible reactions involved in the different mechanisms. From the temperature dependencies of the equilibrium constants, standard reaction enthalpies $\Delta H_{r,m}°$ and entropies $\Delta S_{r,m}°$ can be estimated. For the equilibrium constants K_c of OH addition and decomposition reactions of model-2 and model-3, the following equation applies:

$$K_c = \frac{k_F}{k_R} = \frac{k_B T}{p^\circ} \times \exp\left(\frac{-\Delta H^\circ_{r,m}}{RT} + \frac{\Delta S^\circ_{r,m}}{R}\right) \quad (8)$$

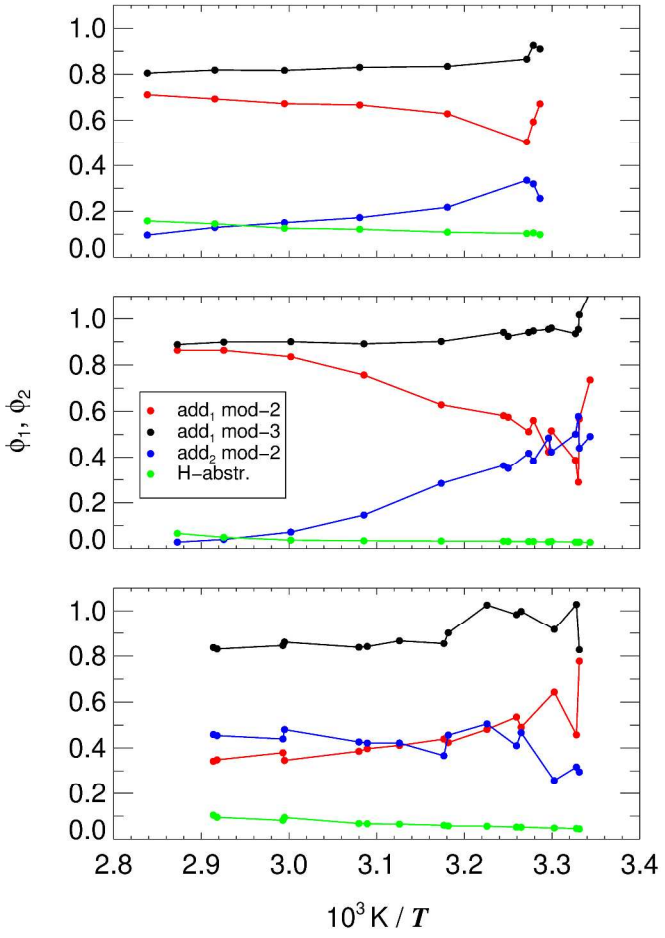

Fig. 7 Yields of add_1 (red) and add_2 (blue) of model-2, add_1 of model-3 (black), and the contribution of H-abstraction (green) following the OH + aromatics reaction for 14-DMB (upper panel), 135-TMB (middle panel), and 1245-TeMB (lower panel).

where k_B is the Boltzmann constant and p° the standard pressure. Because of a simpler stoichiometry, the expression for the isomerization reactions of model-3 is simpler, and the K_i are dimensionless:

$$K_i = \frac{k_F}{k_R} = \frac{k_{12}}{k_{21}} = \exp\left(\frac{-\Delta H^\circ_{r,m}}{RT} + \frac{\Delta S^\circ_{r,m}}{R}\right) \quad (9)$$

Correspondingly, the following simplified functions were fitted to the K_c and K_i, respectively: $K_c = A \times T \times \exp(-B/T)$ and $K_i = A \times \exp(-B/T)$. The ratios k_F/k_R can be calculated from the fit parameters as shown previously[11] for model-2:

$$K_{c1} = \frac{[k_{11a}k_{-11a}]}{(k_{L1} - k_{31})^2} \quad (10)$$

$$K_{c2} = \frac{[k_{12a}k_{-12a}]}{(k_{L2} - k_{32})^2} \quad (11)$$

For model-3, the following equations apply (k_{12} is determined by solving the right hand side of equation (7)):

$$K_{c1} = \frac{[k_{11a}k_{-11a}]}{(k_{L1} - k_{12} - k_{31})^2} \quad (12)$$

$$K_i = \frac{[k_{12}k_{21}]}{(k_{L2} - k_{32})^2} \quad (13)$$

For the K_c and K_i calculations, the rate constants k_{31} and k_{32} that were determined in the last section were used. However, instead of using equations (10)-(13) we followed a slightly different approach and adapted our fit routines to directly return the equilibrium constants. The results are obviously the same but the advantage is that uncertainty estimates for the K_c and K_i can be determined directly by the method described in section 3. Also in this case, these estimates are not considered absolute but suitable to weight the data points in fits of the parameters A and B and their uncertainties with the bootstrap method. However, the uncertainties of the parameters A and B are again lower limits, because the background loss rate constants k_{31} and k_{32}, whose influence is significant at lower temperatures, were held fixed in the analysis. The K_c of model-2 and model-3, and the K_i of model-3 are listed in Table S6 and shown in Figs. 8 and 9, respectively. Parameters A and B and corresponding thermodynamic data are listed in Table 4 including those obtained in the re-evaluation of HMB data[9] and those calculated from k_F and k_R results of benzene by Knispel et al.[4]. For comparison, the K_c functions for benzene and HMB were also included in Fig. 8 as dotted and dashed lines, respectively. Benzene and HMB are compounds for which the underlying mechanism of OH addition is not questioned (model-1). They represent the formation of prototype non-*ipso* adducts with no methylation and *ipso* adducts with full methylation of the aromatic ring, respectively.

The thermodynamic quantities of benzene and HMB clearly show that while reaction entropies are expectedly similar and in a reasonable range for an association reaction, the OH-HMB adduct formation is more exothermic by about −25 kJ mol^{-1}. This is in line with a recently calculated value of the zero-point reaction energy of the OH + HMB addition of –102 kJ mol^{-1} by Loison et al.[10] Moreover, the activation energies of the decomposition reactions of the OH-benzene and OH-HMB adducts (Tab. 3) are in accord with the reaction enthalpies of the forward reactions.

Tab. 4 Parameters A and B and corresponding molar reaction enthalpies $\Delta H_{r,m}°$ and entropies $\Delta S_{r,m}°$ describing equilibrium constants of reversible OH + aromatics reactions according to the equation: $K_c = A \times T \times \exp(-B/T)$ and of adduct isomerization according to the equation: $K_i = A \times \exp(-B/T)$. Error limits do not include potential systematic effects caused by deficiencies of reaction models.

	$\ln(A$ / $K^{-1}cm^3)$	B / 10^3 K	$\Delta S_{r,m}°$ / J K^{-1} mol^{-1}	$\Delta H_{r,m}°$ / kJ mol^{-1}	$\ln(A$ / $K^{-1}cm^3)$, $\ln(A)$	B / 10^3 K	$\Delta S_{r,m}°$ / J K^{-1} mol^{-1}	$\Delta H_{r,m}°$ / kJ mol^{-1}
model-2	OH + aromatic → add_1				OH + aromatic → add_2			
14-DMB	−60.9 ± 0.6	−8.2 ± 0.2	−88 ± 5	−68 ± 2	−64.6 ± 0.6	−9.6 ± 0.2	−119 ± 5	−80 ± 2
135-TMB	−59.6 ± 1.3	−8.3 ± 0.4	−77 ± 11	−69 ± 4	−73.3 ± 0.7	−12.8 ± 0.2	−191 ± 6	−106 ± 2
1245-TeMB	−68.3 ± 2.2	−10.6 ± 0.7	−149 ± 18	−88 ± 6	−62.1 ± 1.8	−9.4 ± 0.6	−98 ± 15	−78 ± 5
model-3	OH + aromatic → add_1				add_1 → add_2			
14-DMB	−63.5 ± 0.4	−9.2 ± 0.1	−109 ± 4	−77 ± 1	−0.03 ± 0.65	0.1 ± 0.2	−0.2 ± 5.4	0.5 ± 1.8
135-TMB	−67.1 ± 0.3	−10.8 ± 0.1	−139 ± 3	−90 ± 1	−2.8 ± 0.6	−0.7 ± 0.2	−23 ± 5	−6 ± 2
1245-TeMB	−63.3 ± 1.9	−9.5 ± 0.6	−108 ± 16	−79 ± 5	−1.95 ± 1.3	−0.9 ± 0.4	−16 ± 11	−8 ± 3
model-1	OH + aromatic → add							
benzene[a]	−64.5 ±1.4	−9.0 ± 0.4	−118 ± 11	−75 ± 4	–	–	–	–
HMB	−65.9 ± 1.1	−12.1 ± 0.4	−130 ± 9	−101 ± 3	–	–	–	–

[a] Evaluated from k_F and k_R data by Knispel et al.,[4] $K_c = k_F/k_R$.

The K_c of all other investigated compounds range between the minimum and maximum values of benzene and HMB. Model differences regarding add_1 are significant, with minimum and maximum K_c corresponding to model-2 and model-3, respectively. On the other hand, model-2 defines the maximum K_c of add_2 that all exceed those of add_1, except for 135-TMB where K_c functions of add_1 and add_2 cross each other. In contrast to the K_c in Fig. 8, the K_i in Fig. 9 show weak, insignificant temperature dependencies for all compounds, indicating comparatively small reaction enthalpies for potential isomerization reactions. Despite these differences between model-2 and model-3, a decision which model is more realistic turns out to be difficult. In the previous investigation on 135-TMB[11] model-3 was favored based on the obtained reaction enthalpies and entropies, in particular because add_2 formation of model-2 was strongly exothermic while the reverse decomposition had a low activation energy. Moreover, the reaction entropy of add_2 formation was much lower than expected.[11] These findings are confirmed in this work for 135-TMB. However, no such inconsistencies of model-2 are evident for 14-DMB and 1245-TeMB. On the other hand, the same is true for model-3: enthalpies and entropies of add_1 formations and isomerization reactions are in a reasonable range for these compounds, at least considering the range spanned by benzene and HMB.

Available theoretical work on OH + aromatics reactions in the literature is based on model-2, i.e. isomerization reactions have not been considered so far. Theoretical studies on the OH + toluene reaction show that adduct isomers benefit energetically from CH_3 substituents in *ortho* and to a lesser extent in *para* position with respect to OH attack.[43,44] Regarding the *ipso* adduct of toluene, predictions are discordant ranging slightly below the *para* or above the *ortho* adduct, but in any case within 10 kJ mol^{-1}.[43,44] Studies by Fan and Zhang on 14-DMB[27] and 13-DMB[28] (four adducts) also report stabilizing effects of CH_3 substituents in *ortho* and *para*, but not in *ipso* positions. This is confirmed qualitatively in work by Huang et al. on 12-DMB[45] and 13-DMB,[46] and in recent work by Pan and Wang on 13-DMB,[47] as well as on *p*-cymene (except for the *ipso* adduct with respect to the C_3H_7 substituent).[12] These theoretical studies also imply that generally *ortho* adducts are formed with greater yields and typically decompose more quickly than *ipso* adducts, despite more exothermic formation enthalpies, i.e. for the compounds studied here add_1 = *ortho* and add_2 = *ipso* is implicated.

If this concept is transferred qualitatively to the selected compounds, one would expect reaction enthalpies *ortho* ≤ *ipso* for 14-DMB, *ortho* < *ipso* for 135-TMB, and *ortho* ≤ *ipso* for 1245-TeMB. Moreover, the *ortho* and *ipso* adduct formation of 135-TMB should be the most and the least exothermic among the six reactions studied. It can also be inferred that the formation of the *ortho* adduct of 135-TMB should be similarly exothermic than that of the *ipso* adduct of HMB that is also stabilized by two CH_3 substituents in *ortho* position and one in *para* position.

In reasonable agreement with these considerations we find relatively high model-2 yields of add_1 and similar reaction enthalpies for add_1 and add_2 formations in the case of 14-DMB and 1245-TeMB. On the other hand, the 135-TMB result of model-2 again does not fit because the formation of the alleged *ipso* adduct add_2 would be more exothermic by −40 kJ mol^{-1} than that of the *ortho* adduct add_1. For model-3 reaction enthalpies of add_1 formations are in the expected range and order for all three compounds with 135-TMB being the most exothermic. However, for 135-TMB the reaction enthalpy of the add_1 → add_2 isomerization is negative by −6 kJ mol^{-1}, again

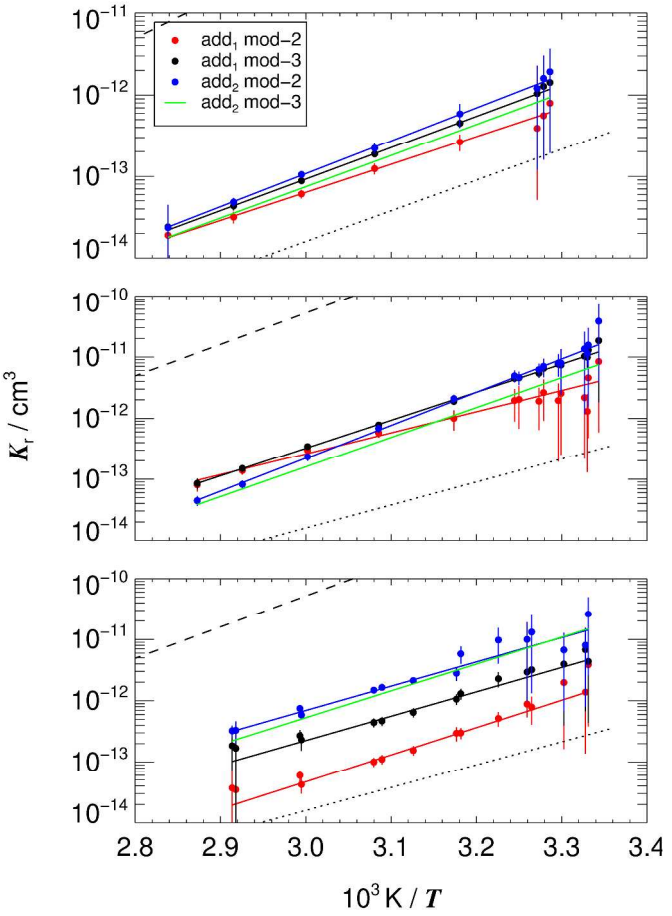

Fig. 8 Van't Hoff plots of equilibrium constants of reversible OH + aromatics reactions for 14-DMB (upper panel), 135-TMB (middle panel) and 1245-TeMB (lower panel). Red: $K_{c1} = k_{11a}/k_{-11a}$ of model-2, blue: $K_{c2} = k_{12a}/k_{-12a}$ of model-2, and black: $K_{c1} = k_{11a}/k_{-11a}$ of model-3. Green lines show the limiting K_{c2} of model-3 according to equation (14), dotted and dashed lines show model-1 results for benzene and HMB for comparison.

indicating an at least slightly more stable *ipso* adduct. An even more exothermic enthalpy for the $add_1 \rightarrow add_2$ reaction was estimated before, albeit with a high uncertainty (−35±22 kJ mol^{-1}).[11] Obviously, neither model-2 nor model-3 is leading to an overall picture that is fully consistent with available theoretical work.

The question remains whether or not the thermodynamic quantities of intermediate cases lie in between those of the limiting models discussed so far or if other results are possible. Because of the degeneracy problem (more fit parameters than parameters describing the decay curves), intermediate cases between model-2 and model-3 are difficult to assess quantitatively. However, a relationship between the three equilibrium constants exists following the detailed balancing applied previously to derive the analytical solutions for the general mechanism:[11]

$$K_i = \frac{K_{c2}}{K_{c1}} = \frac{[k_{12a}k_{-12a}] \times (k_{L1} - k_{12} - k_{31})^2}{[k_{11a}k_{-11a}] \times (k_{L2} - k_{21} - k_{32})^2} \qquad (14)$$

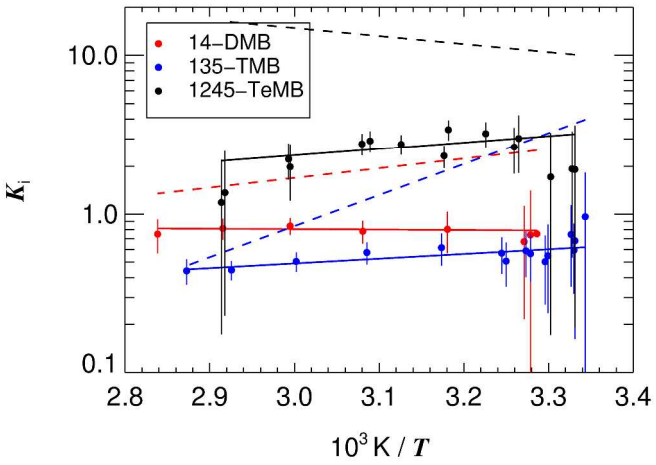

Fig. 9 Van't Hoff plots of equilibrium constants for isomerization $K_i = k_{12}/k_{21}$ of model-3 for 14-DMB (red), 135-TMB (blue), and 1245-TeMB (black). The dashed curves show the calculated, limiting K_i of model-2 according to equation (14).

Note that in terms of equations (8) and (9), the left hand side of equation (14) corresponds to a path-independence of the state-function changes ΔH and ΔS. Inserting $k_{12} = \sqrt{K_i \times [k_{12}k_{21}]}$ and $k_{21} = \sqrt{[k_{12}k_{21}]/K_i}$, a general equation for K_i was obtained:

$$K_i = \frac{\left(\sqrt{[k_{12a}k_{-12a}]} \times k_{L1} + \sqrt{[k_{11a}k_{-11a}] \times [k_{12}k_{21}]} - k_{31} \times \sqrt{[k_{12a}k_{-12a}]}\right)^2}{\left(\sqrt{[k_{11a}k_{-11a}]} \times k_{L2} + \sqrt{[k_{12a}k_{-12a}] \times [k_{12}k_{21}]} - k_{32} \times \sqrt{[k_{11a}k_{-11a}]}\right)^2} \qquad (15)$$

The range of possible K_i was determined in a number of further fits to OH decay curve arrays taking 135-TMB as an example, where the parameter $[k_{12a}\,k_{-12a}]$ was increased stepwise from zero to the maximum value obtained for model-2. Alternatively, the parameter $[k_{12}\,k_{21}]$ could have been decreased from its model-3 maximum down to zero. During these fits, the rate constants k_{31} and k_{32} were held fixed at averaged values, based on the optimized model-2 and model-3 results. It turned out that the K_i indeed change smoothly and that equation (14) also applies to the limiting cases, i.e. a maximum K_i can be calculated for model-2 as well as a minimum K_{c2} for model-3, as indicated by the green and dashed lines in Figs. 8 and 9, respectively. The true equilibrium constants and corresponding thermodynamic data should in any case range within these limits. Accordingly, the true mechanism could lie somewhere between model-2 and model-3.

Conclusions

For seven aromatic compounds slightly negative temperature coefficients were obtained for the total OH rate constants as well as a general tendency towards greater rate

constants with increasing methylation. Both findings are complementary with previous studies. Temperature dependent OH rate constants for the three TeMBs and PMB were determined for the first time. Room temperature rate constants for 1245-TeMB and PMB previously reported in only study[32] were confirmed. All OH rate constants are applicable under atmospheric conditions. Furthermore, a detailed analysis of OH decay curves for three selected compounds revealed insight into the reaction mechanism involving adduct formation, decomposition and possible isomerizations. 14-DMB, 135-TMB and 1245-TeMB were selected because they can form only two adduct isomers: an *ortho* and an *ipso* adduct each. The analysis was based on analytical solutions from a previous study on 135-TMB.[11] The general problem with these solutions is that different mechanisms can lead to the same OH decay curves. Therefore limiting cases of a more general reaction mechanism were examined and the outcome was checked for consistency and qualitative agreement with theoretical predictions from the literature. In summary, adduct yields, reaction entropies and enthalpies obtained in the analysis lie in reasonable ranges for all three compounds. However, the open questions regarding the correct reaction mechanism raised in the previous work on 135-TMB[11] could not be answered here conclusively based on results from two more compounds for which a qualitatively similar mechanism was generally expected. Overall, the reaction model including isomerization led to more conclusive results. Moreover, it was inferred that the *ortho* adducts are those that are formed with higher yields and that decompose more quickly back to OH. To further elucidate the importance of different adduct isomers and the potential role of isomerizations, theoretical studies including the investigated compounds would be helpful. In any case, the rate constants derived for potential isomerization reactions are too slow to be of importance for the atmospheric degradation of the aromatics where a fast reaction of the primarily formed adducts with O_2 is expected. For the same reason the primary yields of adduct isomers are expected to determine the further atmospheric degradation. On the other hand, isomerizations could play a role in laboratory studies at reduced O_2 concentrations or in the absence of O_2.

Acknowledgements

This work was supported by the Deutsche Forschungs-gemeinschaft under grant ZE 792/6-1 and BO 1580/3-1 within the French-German CNRS-INSU/DFG bilateral program ATMOCHEM. We thank MSc Johannes Kaldun and Prof. Matthias Breuning from the Organic chemistry department of the University of Bayreuth for the synthesis of isodurene and the GC-FID analysis of the studied compounds.

Notes and references

[a] *Atmospheric Chemistry Research Laboratory, University of Bayreuth, 95448, Germany.*
[b] *Institut für Energie- und Klimaforschung IEK-8: Troposphäre, Forschungszentrum Jülich, 52425 Jülich, Germany.*
[c] *Fraunhofer Institute for Toxicology and Experimental Medicine, 30625 Hannover, Germany.*
E-mail: b.bohn@fz-juelich.de

†Electronic Supplementary Information (ESI) available. See DOI: 10.1039/b000000x/

1. J. G. Calvert, R. Atkinson, K. H. Becker, R. M. Kamens, J. H. Seinfeld, T. J. Wallington and G. Yarwood, *The Mechanism of Atmospheric Oxidation of Aromatic Hydrocarbons*, Oxford University Press, New York, 2002.
2. R. Atkinson, *J. Phys. Chem. Ref. Data. Monograph 1*, 1989.
3. R. Atkinson and J. Arey, *Chem. Rev.*, 2003, **103**, 4605-4638.
4. R. Knispel, R. Koch, M. Siese and C. Zetzsch, *Ber. Bunsenges. Phys. Chem*, 1990, **94**, 1375-1379.
5. R. Koch, R. Knispel, M. Elend, M. Siese and C. Zetzsch, *Atmos. Chem. Phys.*, 2007, **7**, 2057-2071.
6. A. Wahner and C. Zetzsch, *J. Phys. Chem.*, 1983, **87**, 4945-4951.
7. R. Koch and C. Zetzsch, First experimental evidence of ipso-addition of OH to methyl-substituted aromatics and O2 reactivity of hexamethylbenzene–OH, Bunsentagung Erlangen, 2006.
8. T. Berndt and O. Böge, *Int. J. Chem. Kinet.*, 2001, **33**, 124-129.
9. J. von Buttlar, R. Koch, M. Siese and C. Zetzsch, *Geophysical Research Abstracts*, 2008, **10**, EGU2008-A-10576.
10. J.-C. Loison, M.-T. Rayez, J.-C. Rayez, A. Gratien, P. Morajkar, C. Fittschen and E. Villenave, *J. Phys. Chem. A*, 2012, **116**, 12189-12197.
11. B. Bohn and C. Zetzsch, *Phys. Chem. Chem. Phys.*, 2012, **14**, 13933-13948.
12. P. Alarcon, B. Bohn, C. Zetzsch, M. T. Rayez and J. C. Rayez, *Phys. Chem. Chem. Phys.*, 2014, **16**, 17315-17326.
13. P. Alarcon, R. Strekowski and C. Zetzsch, *Phys. Chem. Chem. Phys.*, 2013, **15**, 20105-20114.
14. S. Zhang, R. Strekowski, L. Bosland, A. Monod and C. Zetzsch, *Phys. Chem. Chem. Phys.*, 2011, **13**, 11671 - 11677.
15. S. Zhang and C. Zetzsch, 21th International Symposium on Gas Kinetics 2010, Leuven, Belgium.
16. A. Bolovinos, J. Philis, E. Pantos, P. Tsekeris and G. Andritsopoulos, *The Journal of Chemical Physics*, 1981, **75**, 4343-4349.
17. A. Bolovinos, J. Philis, E. Pantos, P. Tsekeris and G. Andritsopoulos, *Journal of Molecular Spectroscopy*, 1982, **94**, 55-68.
18. S. P. Sander, J. Abbatt, J. R. Barker, J. B. Burkholder, R. R. Friedl, D. M. Golden, R. E. Huie, C. E. Kolb, M. J. Kurylo, G. K. Moortgat, V. L. Orkin and P. H. Wine, *Chemical kinetics and photochemical data for use in atmospheric studies, Evaluation No. 17, Jet Propulsion Laboratory, Pasadena, 2011,* http://jpldataeval.jpl.nasa.gov, 2011.
19. L. I. Smith, *Organic Syntheses*, 1931, **11**, 66.
20. R. A. Perry, R. Atkinson and J. N. Pitts, *J. Phys. Chem.*, 1977, **81**, 296-304.
21. F. Witte, E. Urbanik and C. Zetzsch, *J. Phys. Chem.*, 1986, **90**, 3251-3259.
22. H. Geiger, I. Barnes, K. Becker, B. Bohn, T. Brauers, B. Donner, H.-P. Dorn, M. Elend, C. Freitas Dinis, D. Grossmann, H. Hass, H. Hein, A. Hoffmann, L. Hoppe, F. Hülsemann, D. Kley, B. Klotz, H. Libuda, T. Maurer, D. Mihelcic, G. Moortgat, R. Olariu, P. Neeb, D. Poppe, L. Ruppert, C. Sauer, O. Shestakov, H. Somnitz, W. Stockwell, L. Thüner, A. Wahner, P. Wiesen, F. Zabel, R. Zellner and C. Zetzsch, *J. Atmos. Chem.*, 2002, **42**, 323-357.
23. A. C. Davison and D. V. Hinkley, *Bootstrap methods and their application*, Cambridge University Press, Cambridge ; New York, NY, USA, 1997.

24. I. Suh, D. Zhang, R. Zhang, L. T. Molina and M. J. Molina, *Chem. Phys. Lett*, 2002, **364**, 454-462.
25. L. J. Bartolotti and E. O. Edney, *Chemical Physics Letters*, 1995, **245**, 119-122.
26. V. H. Uc, I. García-Cruz, A. Hernández-Laguna and A. Vivier-Bunge, *J. Phys. Chem. A*, 2000, **104**, 7847-7855.
27. J. Fan and R. Zhang, *J. Phys. Chem. A*, 2006, **110**, 7728-7737.
28. J. Fan and R. Zhang, *J. Phys. Chem. A*, 2008, **112**, 4314-4323.
29. J. M. Andino, J. N. Smith, R. C. Flagan, W. A. Goddard and J. H. Seinfeld, *The Journal of Physical Chemistry*, 1996, **100**, 10967-10980.
30. D. Mehta, A. Nguyen, A. Montenegro and Z. Li, *J. Phys. Chem. A*, 2009, **113**, 12942-12951.
31. S. M. Aschmann, W. D. Long and R. Atkinson, *J. Phys. Chem. A*., 2006, **110**, 7393-7400.
32. S. M. Aschmann, J. Arey and R. Atkinson, *J. Phys. Chem. A*, 2013, **117**, 2556-2568.
33. D. A. Hansen, R. Atkinson and J. N. Pitts, *J. Phys. Chem*., 1975, **79**, 1763-1766.
34. G. J. Doyle, A. C. Lloyd, K. R. Darnall, A. M. Winer and J. N. Pitts, *Environ. Sci. Technol.*, 1975, **9**, 237-241.
35. A. R. Ravishankara, S. Wagner, S. Fischer, G. Smith, R. Schiff, R. T. Watson, G. Tesi and D. D. Davis, *Int. J. Chem. Kinet.*, 1978, **10**, 783-804.
36. J. M. Nicovich, R. L. Thompson and A. R. Ravishankara, *J. Phys. Chem.*, 1981, **85**, 2913-2916.
37. T. Ohta and T. Ohyama, *B. Chem. Soc. Jpn*, 1985, **58**, 3029-3030.
38. E. O. Edney, T. E. Kleindienst and E. W. Corse, *Int. J. Chem. Kinet.*, 1986, **18**, 1355-1371.
39. R. Atkinson and S. M. Aschmann, *Int. J. Chem. Kinet.*, 1989, **21**, 355-365.
40. R. Sommerlade, H. Parlar, D. Wrobel and P. Kochs, *Environ. Sci. Technol.*, 1993, **27**, 2435-2440.
41. F. Kramp and S. E. Paulson, *J. Phys. Chem. A*, 1998, **102**, 2685-2690.
42. S. M. Aschmann, E. C. Tuazon and R. Atkinson, *J. Phys. Chem. A*., 2005, **109**, 2282-2291.
43. J. M. Andino and A. Vivier-Bunge, *Advances in Quantum Chemistry*, 2008, **55**, 297-310.
44. R. Wu, S. Pan, Y. Li and L. Wang, *The Journal of Physical Chemistry A*, 2014, **118**, 4533-4547.
45. M. Huang, W. Zhang, Z. Wang, L. Hao, W. Zhao, X. Liu, B. Long and L. Fang, *Int. J. Quant. Chem.*, 2008, **108**, 954-966.
46. M. Q. Huang, Z. Y. Wang, L. Q. Hao and W. J. Zhang, *Comput Theor Chem*, 2011, **965**, 285-290.
47. S. Pan and L. Wang, *The Journal of Physical Chemistry A*, 2014, **118**, 10778-10787.

